PERGAMON

International Journal of Heat and Mass Transfer 43 (2000) 3811–3822

International Journal of HEAT and MASS TRANSFER

www.elsevier.com/locate/ijhmt

# Simulation of coupled turbulent flow and heat transfer in the wedge-shaped pool of a twin-roll strip casting process

Woo-Seung Kim[a,*], Deok-Soo Kim[b], A.V. Kuznetsov[c]

[a]*Department of Mechanical Engineering, Hanyang University, 1271 Sa 1-dong, Ansan-si, Kyunggi-do 425-791, South Korea*
[b]*Department of Mechanical Engineering, Hanyang University, Seoul 133-791, South Korea*
[c]*Department of Mechanical and Aerospace Engineering, North Carolina State University, Raleigh, NC 27695, USA*

Received 1 July 1999; received in revised form 10 December 1999

**Abstract**

The proper choice of nozzle in a twin-roll strip casting process is important to obtain the stabilization of the molten steel and free surface and a stable temperature distribution in a wedge-shaped pool. In this study, a numerical investigation of the coupled turbulent flow and heat transfer in a twin-roll strip casting process was performed for two patterns of melt-feed through a nozzle. In addition, the patterns for the removal of superheat for different gap thicknesses were analyzed using a local Nusselt number along the roll surface. The flow turbulence was examined using the low-Reynolds-number $k$–$\varepsilon$ turbulence model of Launder and Sharma. The results show that the use of a submerged nozzle may have a beneficial impact on the stabilization of the free-surface zone. The increased gap thickness yields an increased local Nusselt number in the downstream section of the wedge-shaped pool where the cross-sectional flow area is reduced. 

## 1. Introduction

Facing stiff competition in the international market, steel manufacturers have been driven to simplify conventional operational procedures, increase productivity, and reduce energy consumption in their primary manufacturing processes. There has been considerable interest in the development of a new generation of casting equipment, which would economically produce near-net-shaped casts such as thin slab, strip, and thin strip [1–5]. The twin-roll strip caster is one of these near-net-shaped casters that has received increased attention in the steel industry. The twin-roll strip caster produces a thin strip through the rapid solidification of molten steel as it is fed through a nozzle from a tundish into a wedge-shaped pool, composed of a couple of cooling rolls and two side-dams.

In the direct production of a thin strip from molten steel, the melt fed through the nozzle from the tundish affects the flow patterns and the characteristics of heat transfer in the pool. The various defects associated with this transport phenomena in the pool, such as break-out, free-surface waves, ripple marks, etc., can reduce casting process efficiency and adversely impact product functionality.

Another problem is that the flow of molten steel in twin-roll strip casting processes can be turbulent; thus the selection of the appropriate process conditions and parameters requires a fundamental understanding and application of the transport phenomena of fluid flow and heat transfer in these processes.

* Corresponding author. Tel.: +82-345-400-5248; fax: +82-345-418-0153.
*E-mail address:* wskim@email.hanyang.ac.kr (W.-S. Kim).

0017-9310/00/$ - see front matter 
PII: S0017-9310(00)00013-2

**Nomenclature**

| | |
|---|---|
| $c_p$ | specific heat |
| $D$ | width of inlet nozzle |
| $h$ | time-averaged enthalpy ($c_pT$) or averaged heat transfer coefficient |
| $h_\xi$, $h_\eta$ | geometrical coefficients, $h_\xi=(x_\xi^2+y_\xi^2)^{1/2}$, $h_\eta=(x_\eta^2+y_\eta^2)^{1/2}$ |
| $J$ | Jacobian |
| $k$ | turbulent kinetic energy |
| $K$ | conductivity |
| mpm | meter per minute |
| $P$ | time-averaged pressure |
| $Re_t$ | turbulent Reynolds number ($\rho k^2/\mu\varepsilon$) |
| $s$ | distance along the roll surface from free surface |
| $S$ | total contact length between melt and roll or source term |
| $t$ | gap thickness |
| $T$ | time-averaged temperature |
| $u_i$ | time-averaged velocity in the $i$ direction |
| $u$, $v$ | time-averaged velocities in the $x$, $y$ directions |
| $u_\xi$, $u_\eta$ | covariant velocity components |
| $U$, $V$ | contravariant velocity components |
| $x_i$ | coordinate in the $i$ direction |

*Greek symbols*

| | |
|---|---|
| $\xi$, $\eta$ | transformed coordinates |
| $\alpha_\xi$, $\alpha_\eta$ | geometrical coefficients, $\alpha_\xi=h_\xi h_\eta^2/J$, $\alpha_\eta=h_\eta h_\xi^2/J$ |
| $\beta_\xi$, $\beta_\eta$ | geometrical coefficients, $\beta_\xi=\lambda h_\eta/J$, $\beta_\eta=\lambda h_\xi/J$ |
| $\varepsilon$ | rate of dissipation of turbulent kinetic energy |
| $\Gamma$ | diffusion coefficient of $\phi$ |
| $\mu$ | laminar viscosity |
| $\phi$ | general dependent variable |
| $\rho$ | density |
| $\sigma_t$ | turbulent Prandtl number |

*Subscripts*

| | |
|---|---|
| in | inlet of nozzle |
| liq | liquidus line |
| r | surface of roll |
| t | turbulence |

Most of the previous work on rapid solidification has used a one-dimensional solidification analysis [6] (based on an analytical approach) or an investigation of the solidification and flow of molten steel with consideration for the flow of the liquid and solid state melt [7–14]. The majority of work on the flow analysis for molten steel has been carried out with the assumption of laminar flow. Although recent work reported by Seyedein and Hasan [15] considered the turbulent characteristics of the flow, the analysis was carried out for the unrealistic strip thicknesses of 20–40 mm. These thicknesses are much thicker than those formed in the actual strip casting processes. Thus, the corresponding results of the process conditions used in these previous studies tend to be unrealistic.

Although the investigations of twin-roll casting processes with the ability of continuous, direct production of near-net-shaped strip from melt have been performed, the quantitative relationships between process parameters, such as the feeding temperature of the melt, the casting speed, the gap thicknesses, the melt-feed types, etc., have not been examined carefully. In particular, few studies of the characteristics of fluid flow and heat transfer in conjunction with the feed patterns of the melt through a submerged nozzle have appeared in open literature. Moreover, the corresponding control techniques for these characteristics have yet to be established.

An investigation of the submerged nozzle is necessary because the appropriate choice of a submerged nozzle type, related to the characteristics of the flow and heat transfer in the pool, plays a critical role in the twin-roll strip casting process.

The present work is a numerical investigation of the characteristics of the fluid flow and heat transfer in a wedge-shaped pool during the strip casting process. The purpose of this study is to develop a fundamental understanding of how to design a twin-roll casting system that will produce a near-net-shaped strip, in connection with the melt-feed type through a submerged nozzle. A primary goal of this study is to investigate the characteristics of the turbulent flow and heat transfer in a system that feeds the melt through a submerged nozzle into a wedge-shaped pool. Furthermore, the effects of roll gap thicknesses on the flow pattern of melt and on the temperature distribution are investigated for this numerical model. Then, based on the corresponding results, the patterns of superheat removal are estimated.

## 2. Theory

### 2.1. Mathematical model

A schematic diagram of a twin-roll strip casting system is shown in Fig. 1. Molten steel is supplied continuously, with a constant mass flow rate, through a nozzle from a tundish into a wedge-shaped pool. The molten steel is quenched by a couple of cooling rolls which rotate

in opposing directions. The tangential velocities of these roll surfaces are equal to the casting speed. In general, the Reynolds number of the melt flow fed through the nozzle into the pool is of the order of $10^3$–$10^4$. The roll surface temperature is assumed to be the liquidus temperature. This allows for the estimation of the amount of superheat removed by the cooling rolls. The estimation of the superheat removal for the liquid-state steel is valid because the solidified shell and mushy layers which form on the roll surface during the strip casting process are very thin [15]. In considering the complex flow patterns in the twin-roll strip casting processes, the transport equation should include the effects of the turbulence. The turbulent effects were considered [15] using the low-Reynolds-number $k$–$\varepsilon$ turbulence model of Launder and Sharma [16]. The following time-averaged governing equations are utilized in this study:

Continuity equation

$$\frac{\partial u_i}{\partial x_i} = 0 \tag{1}$$

Momentum equation

$$\frac{\partial(\rho u_j u_i)}{\partial x_j} = -\frac{\partial P}{\partial x_i} + \frac{\partial}{\partial x_j}\left[(\mu+\mu_t)\frac{\partial u_i}{\partial x_j}\right] + \frac{\partial}{\partial x_j}\left(\mu_t\frac{\partial u_j}{\partial x_i}\right) - \frac{2}{3}\rho\frac{\partial k}{\partial x_i}\delta_{ij} \tag{2}$$

Energy equation

$$\frac{\partial(\rho u_j h)}{\partial x_j} = \frac{\partial}{\partial x_j}\left[\left(\frac{K}{c_p}+\frac{\mu_t}{\sigma_t}\right)\frac{\partial h}{\partial x_j}\right] \tag{3}$$

Kinetic energy equation

$$\frac{\partial(\rho u_j k)}{\partial x_j} = \frac{\partial}{\partial x_j}\left[\left(\mu+\frac{\mu_t}{\sigma_k}\right)\frac{\partial k}{\partial x_j}\right] + P_t - \rho\varepsilon - D_k \tag{4}$$

Dissipation rate of kinetic energy equation

$$\frac{\partial(\rho u_j \varepsilon)}{\partial x_j} = \frac{\partial}{\partial x_j}\left[\left(\mu+\frac{\mu_t}{\sigma_\varepsilon}\right)\frac{\partial \varepsilon}{\partial x_j}\right] + C_{\varepsilon 1} f_1 P_t \frac{\varepsilon}{k} - C_{\varepsilon 2} f_2 \rho \frac{\varepsilon^2}{k} + E_\varepsilon \tag{5}$$

where

$$\mu_t = C_\mu f_\mu \rho \frac{k^2}{\varepsilon} \tag{6a}$$

$$P_t = \mu_t\left(\frac{\partial u_i}{\partial x_j}+\frac{\partial u_j}{\partial x_i}\right)\frac{\partial u_i}{\partial x_j} \tag{6b}$$

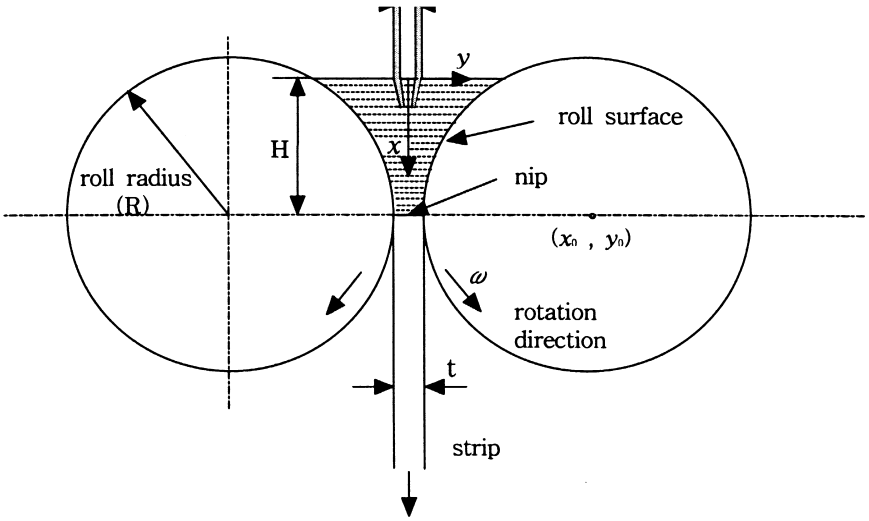


Fig. 1. Schematic diagram of a twin-roll strip caster.

$$D_k = 2\mu \frac{\partial \sqrt{k}}{\partial x_i} \frac{\partial \sqrt{k}}{\partial x_i} \tag{6c}$$

$$E_\varepsilon = \frac{2\mu\mu_t}{\rho} \frac{\partial^2 u_i}{\partial x_j \partial x_k} \frac{\partial^2 u_i}{\partial x_j \partial x_k} \tag{6d}$$

$$f_1 = 1, \quad f_2 = 1 - 0.3 \cdot \exp\left(-Re_t^2\right)$$

$$f_\mu = \exp\left(-3.4/(1 + Re_t/50)^2\right), \quad Re_t = \frac{\rho k^2}{\mu\varepsilon} \tag{6e}$$

$$C_\mu = 0.09,\ C_{\varepsilon 1} = 1.44,\ C_{\varepsilon 2} = 1.92,\ \sigma_k = 1.0,\ \sigma_\varepsilon = 1.3,\ \sigma_t = 0.9 \quad i, j = 1 \text{ or } 2$$

### 2.2. Transformation of coordinates

Because of the complexity of the domain of interest, the governing equations are transformed into general curvilinear coordinates $(\xi, \eta)$. The following transformation of coordinates is introduced:

$$x = x(\xi, \eta), \quad y = y(\xi, \eta) \tag{7}$$

Upon the transformation of coordinates, the governing equations with the general dependent variable, $\phi$, defined in the computational domain, become:

$$\frac{\partial}{\partial \xi}\left(\rho U\phi - \frac{\alpha_\xi \Gamma}{h_\xi}\frac{\partial \phi}{\partial \xi}\right) + \frac{\partial}{\partial \eta}\left(\rho V\phi - \frac{\alpha_\eta \Gamma}{h_\eta}\frac{\partial \phi}{\partial \eta}\right)$$

$$= JS(\xi, \eta) - \frac{\partial}{\partial \xi}\left(\frac{\beta_\xi \Gamma}{h_\eta}\frac{\partial \phi}{\partial \eta}\right) - \frac{\partial}{\partial \eta}\left(\frac{\beta_\eta \Gamma}{h_\xi}\frac{\partial \phi}{\partial \xi}\right) \tag{8}$$

where

$$U = \alpha_\xi u_\xi - \beta_\xi u_\eta \qquad V = \alpha_\eta u_\eta - \beta_\eta u_\xi$$

$$u_\xi = (x_\xi u + y_\xi v)/h_\xi \qquad u_\eta = (x_\eta u + y_\eta v)/h_\eta \tag{9}$$

Other geometrical coefficients are defined in the nomenclature. In Eq. (8), $\phi$ represents $u_\xi$, $u_\eta$, $h$, $k$, and $\varepsilon$, defined in new general coordinates.

### 2.3. Boundary conditions

Only the right half of the region was chosen as the computational domain in the present study because the pool of the twin-roll strip caster, shown in Fig. 1, is assumed to be symmetric with respect to the $x$-axis (casting direction).

#### 2.3.1. Inlet of the nozzle

The dependent variables at the nozzle inlet are assumed to be constant. The values of $k$ and $\varepsilon$ are based on the following semi-empirical expressions suggested by Lai et al. [17], and used in [15]:

$$u = u_{in}, \quad v = 0, \quad h = h_{in}, \quad k = 0.01u_{in}^2, \quad \varepsilon = C_\mu k^{1.5}/0.05/D \tag{10a}$$

#### 2.3.2. Symmetric line

The velocity component normal to the symmetric line, $y = 0$, is zero and the normal gradients of the dependent variables, except for the velocity, are zero. Hence:

$$\frac{\partial u}{\partial y} = \frac{\partial h}{\partial y} = \frac{\partial k}{\partial y} = \frac{\partial \varepsilon}{\partial y} = v = 0 \tag{10b}$$

#### 2.3.3. Free surface

The same boundary conditions that are used along the symmetry line are utilized at the free-surface, $x = 0$. The surface tension effect is not considered on the basis of previous literature [15].

$$\frac{\partial v}{\partial x} = \frac{\partial h}{\partial x} = \frac{\partial k}{\partial x} = \frac{\partial \varepsilon}{\partial x} = u = 0 \tag{10c}$$

#### 2.3.4. Roll surface

The no-slip condition is utilized at the roll surface using the casting speed. It was assumed that the turbulent kinetic energy, $k$, and the rate of dissipation of turbulent kinetic energy, $\varepsilon$, are zero and that the liquidus temperature is maintained on the roll surface [15]. Hence:

$$u = -(y - y_0)\omega, \quad v = (x - x_0)\omega, \quad h = h_{liq}, \quad k = \varepsilon = 0 \tag{10d}$$

#### 2.3.5. Outlet (nip)

The outlet is selected to be 0.385 m from the free surface. The melt flow and temperature at the outlet are assumed to be fully developed. All of the dependent variables have the zero normal gradient as follows:

$$\frac{\partial u}{\partial x} = \frac{\partial v}{\partial x} = \frac{\partial h}{\partial x} = \frac{\partial k}{\partial x} = \frac{\partial \varepsilon}{\partial x} = 0 \tag{10e}$$

### 2.4. Numerical procedure

In conjunction with the feed of molten steel through

a submerged nozzle, the nozzles of the vertical slit entry (Type A) and bifurcated slit entry (Type B) are considered in order to investigate the characteristics of fluid flow and heat transfer in the wedge-shaped pool. The computational domain and the grid system, generated by the algebraic grid generation method, including the shape of the nozzle Type A and Type B, are shown in Fig. 2. The non-uniform mesh systems with $65 \times 53$ and $65 \times 65$ grids, based on previous work [15], are used for nozzle Types A and B, respectively.

The control-volume-based finite difference method is used to discretize the general governing Eq. (8) with general dependent variables. The hybrid scheme for the discretization of convective terms is used and the SIMPLER algorithm of Patankar [18] is used to solve the discrete equations. The general form of the algebraic equation after the discretization of Eq. (8) is as follows:

$$a_P\phi_P = a_E\phi_E + a_W\phi_W + a_N\phi_N + a_S\phi_S + b_\phi \tag{11}$$

where the subscript, P, represents the nodal point at which the computation of physical quantity, $\phi$, is done. E, W, N, and S represent the nodal points around the nodal point, P. $a_E$, $a_W$, $a_N$, and $a_S$ represent the link coefficients, and $b_\phi$ is the local source term. The algebraic equation obtained by the discretization of the governing equation with the specified boundary conditions is solved, iteratively, using the TDMA approach based on the line-by-line method. The following convergence criteria is used in this study:

$$\left|\frac{R_i^{m+1} - R_i^m}{R_i^m}\right| \leq \varepsilon \tag{12}$$

where the superscripts, $m + 1$ and $m$, represent the step of iterative computation, and the subscript, $i$, represents the nodal point at which the physical amount is calculated. $R$ is a residual and $\varepsilon$ is a convergence criterion. The value of $\varepsilon$ in this study is taken to be $10^{-5}$. The computation is terminated when Eq. (12) is satisfied for all the computed values of the variables. The underrelaxation factors, 0.4 and 0.25, are used for the velocities and scalar quantities, respectively.

## 3. Results and discussion

The geometrical data for the physical domain of interest and the thermophysical properties of the melt, used in the present simulation, are listed in Table 1. In general, the casting speeds for the twin-roll strip casting processes may be chosen on the basis of the various process parameters such as roll gap thickness, the material of roll, the feed temperature of the melt, the depth of the pool, the amount of cooling water to the roll, and so on. Among those parameters, the range of speeds of 20–110 mpm (0.3–1.8 m/s) was chosen, depending mainly on the roll gap thickness and the

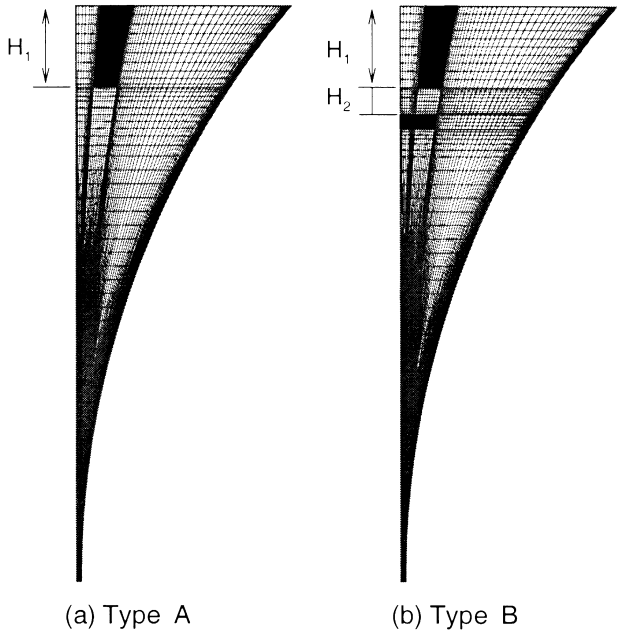


Fig. 2. Computational domain with grid configuration and nozzle shape: (a) Type A: $65 \times 53$ grid, (b) Type B: $65 \times 65$ grid.

amount of the cooling water to the roll. By selecting a casting speed of 60 mpm (1 m/s), the effects of the various roll gap thicknesses on the melt flow pattern and temperature field in the pool and the characteristics of heat transfer at the roll surface are investigated. The inlet velocity of the nozzle is calculated on the basis of the mass balance between inlet and outlet. The superheat of the melt is 20°C.

In Fig. 3, the flow patterns are shown for the submerged entry nozzle with the slit-shaped nozzle exit in different directions. For the typical melt-feed-types applied to the twin-roll strip caster, the case of the single nozzle exit (Type A) toward the outlet is shown in Fig. 3(a), and the case of the bifurcated entry (Type B) toward the cooling roll is shown in Fig. 3(b). The right part of the symmetric line shows the velocity vectors and the left one shows the streamlines.

As shown in Fig. 3(a) for the single exit nozzle, the melt flow injected from the nozzle is weakening during the approach to the outlet as the cross-sectional area of the flow reduces. It also forms the flow exiting the outlet and the flow toward the free surface. A part of the flow toward the free surface gradually moves toward the roll due to the influence of the shear flow formed by the rotating roll [15]. The flow which approaches the free surface forms both the flow toward the nozzle and the roll. As can be seen from Fig. 3(a), the forced flow of the melt through the nozzle and the shear flow formed by the rotating rolls form strongly counter-rotating recirculating flows by their interactions. Fig. 3(b) for the bifurcated entry shows that the jet flow from the nozzle impinges on the roll surface and thereafter forms a flow upstream and downstream toward the free surface and the outlet, respectively. In contrast with Fig. 3(a), the recirculating flows shown in the upper and lower part of nozzle exit are generated mainly by the forced flow of the molten liquid, while the recirculating flow due to the rotating roll is formed around the roll surface, close to the free surface.

As can be observed from the velocity vectors in Fig. 3(a) and (b), the free surface region between the nozzle and the roll is characterized by small flow velocities as compared to the rest of computational domain. The momentum boundary layer thickness developed along the roll surface is shown to be thin in the upper region and thick in the lower region. These results show a contrast to those of Seyedein and Hasan [15] who investigated the case of a direct feed of melt onto the free surface with a non-submerged nozzle. Although a figure for an explicit comparison of the present velocity vectors for a submerged nozzle with those of Seyedein and Hasan [15] is not given in this paper, it was noticed that near the free surface, the velocity vectors with respect to the overall velocity field were shown to be small, compared to those of Seyedein and Hasan [15].

The temperature distribution for the nozzle displayed in Fig. 3 is shown in Fig. 4. The isotherms are plotted in increments of 1°C between 1464 and 1473°C. Fig. 4 shows that the isotherms in the shear flow region have a one-dimensional distribution parallel to the rotational direction of roll. Fig. 4(a) shows that the isotherms are nearly vertical and as can be seen from the velocity vectors in Fig. 3(a), the weak-forced-convection effects appear in the upper region between the nozzle and roll. It is also shown by the streamlines in Fig. 3(a) that as a result of the shear flow due to the roll, a relatively high temperature gradient (circular symbol, P in Fig. 4(a)) appears near the roll surface. Fig. 4(b) shows that in the upper region, the temperature distribution is heavily influenced by the forced convection.

The streamline contours for the different gap thicknesses, in the case of nozzle Types A and B, are shown in Figs. 5 and 6, respectively. These figures make it possible to gain an insight into the effects of the different gap thicknesses on the flow pattern in the pool. It can be seen that an increased gap thickness results in an increase in the intensity of the recirculating flow in the pool. This is due to the fact that for a fixed inlet, an increase in gap thickness leads to an increase in mass flow, resulting in an increase of mass flow in the pool. An increase in the gap thickness is also responsible for the reduction of the recirculating flow zone, due to the forced melt flow supplied through the nozzle, and the recirculating flow zone owing to the rotating rolls is increased. This tendency is especially apparent in Fig. 5 for nozzle Type A. In the case of Fig. 5(a), the recirculating flow regime, which covers an area from the free surface near the nozzle to the middle of the pool, decreases as the gap thickness

Table 1
Physical properties of stainless steel and the geometric data used for the simulation

| Variables | Value |
|---|---|
| Viscosity | 0.007 kg/m/s |
| Density | 0.007 kg/m$^3$ |
| Specific heat | 700 J/kg/K |
| Thermal conductivity | 31 W/m/K |
| Liquidus temperature | 1454°C |
| Inlet temperature | 1474°C |
| Roll diameter | 1.2 m |
| Pool depth ($H$) | 0.385 m |
| Gap thickness | 6–10 mm |
| Inlet width ($D$) | 0.034 m |
| Casting speed | 60 mpm (1 m/s ) |
| Nozzle depth ($H_1$) | 0.055 m |
| Height of nozzle exit ($H_2$) | 0.0184 m |

increases. Fig. 5 also shows that the flow region, descending from the free surface along the nozzle wall, decreases as the gap thickness increases, especially in the upper region near the nozzle, and in Fig. 5(c), it hardly appears at all. In Fig. 6 for the Type B nozzle, with the gap thicknesses increased, the variation of recirculating flow zone is not noticeable. It is also observed here that the recirculating flow region under the nozzle decreases slightly, while the recirculating flow region at the roll surface of the upper pool conversely increases.

The quantitative investigation of turbulence levels in the pool was performed for each of the nozzle types and the non-dimensional turbulent viscosity ($\mu_t/\mu$) distributions are shown in Fig. 7 for a gap thickness of 10 mm. In Fig. 7(a), the maximum value of non-dimensional turbulent viscosity exists in the mid-pool, and the viscosity values in the upper free-surface region are small compared to those in the center of the pool. In Fig. 7(b) (Type B nozzle), the center region of pool just below the submerged nozzle has the highest value of non-dimensional turbulent viscosity, while a high gradient of viscosity appears in the region where the jet flow of melt impinges on the roll. The turbulent viscosity values in the upper free-surface region are smaller than those in the middle of the pool as in Fig. 7(a). Although not shown in this paper, it was known from the observation of the variation of turbulent viscosity for the different gap thicknesses (6 mm, 8 mm, 10 mm) that small gap thicknesses (6 mm, 8 mm) provides smaller predicted turbulent viscosities than those for the large gap thickness (10 mm), though the overall distribution pattern of turbulent viscosity is almost similar to the one in Fig. 7. In the turbulent viscosity distribution of the pool, the results with a non-submerged nozzle, provided by Seyedein and Hasan [15], show very large values of viscosity, covering a zone from the free surface to the center of pool. Comparison of the results in Fig. 7 with those of Seyedein and Hasan [15] with a non-submerged nozzle (not included in this paper) shows that the feed of melt through a submerged nozzle provides a more stable flow pattern in the free surface region of the upper pool than that through a non-submerged nozzle.

The effects of different gap thicknesses on the temperature profile for nozzle Types A and B are shown in Figs. 8 and 9, respectively. The isotherms are presented in equal increments of 1°C between 1464 and 1473°C. The increase in gap thickness, which results in an increasing mass flow into the pool, leads to the

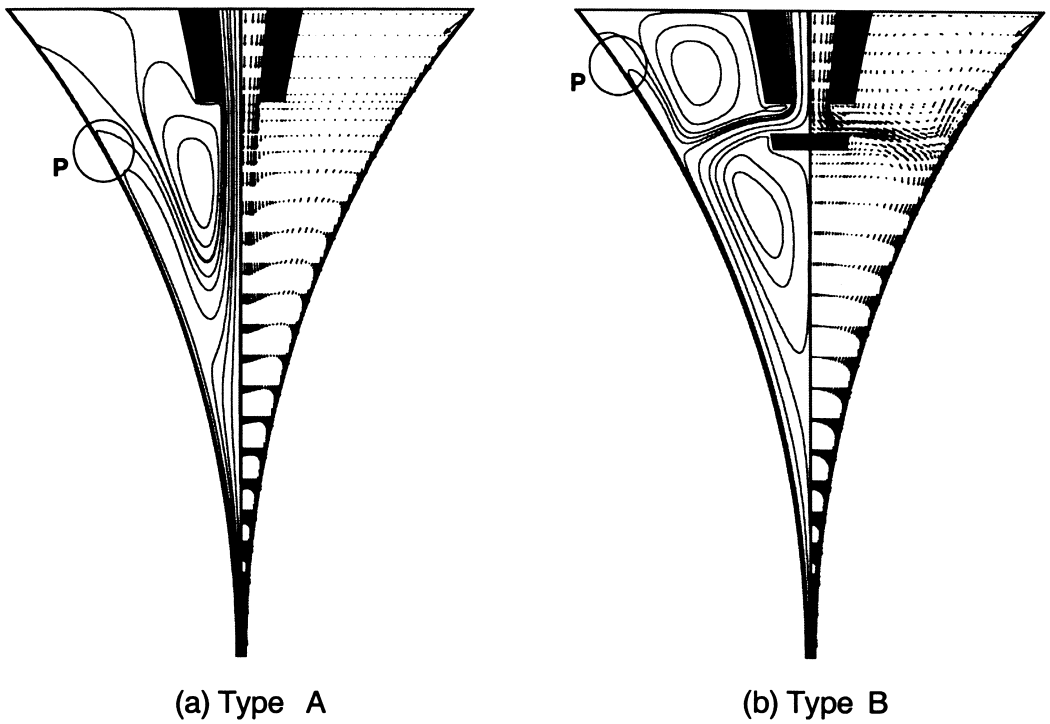


Fig. 3. Velocity vectors and streamlines for gap thickness of 6 mm: (a) Type A, (b) Type B.

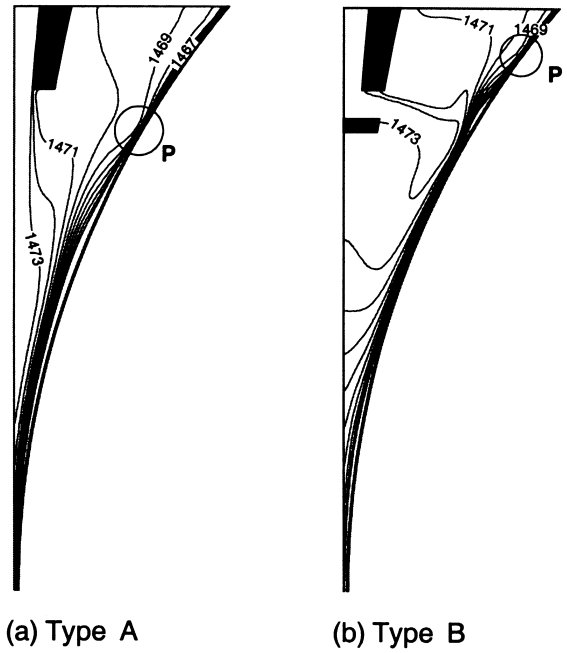


Fig. 4. Isotherms for gap thickness of 6 mm: (a) Type A, (b) Type B.

movement of the isotherms of the upper mid-pool region toward the nozzle. This results in a slight reduction of temperature in the upper pool. On the other hand, there is a very slight movement of isotherms toward the roll surface throughout the mid-pool and the outlet where the cross-sectional area of flow reduces. For the Type A nozzle it is shown that the isotherm patterns, which extend from the free surface to the downstream outlet, remain almost unchanged. The temperature distributions in Figs. 8 and 9 show that the temperature gradient along the free surface boundary is very small. Because of this the surface-tension effect due to the temperature gradient may be neglected for the free surface region. Furthermore, the results for the Type B nozzle shown in Fig. 9 show a slightly higher temperature at the free surface than for the Type A nozzle shown in Fig. 8. Therefore, it is expected that the Type B nozzle has advantages to the Type A nozzle for the prevention of the skull formation at the free surface level. The results of Seyedein and Hasan [15] for a non-submerged nozzle show that the effects of the different gap thicknesses on the temperature distribution are relatively small compared to the present results.

The local heat transfer coefficient on the roll surface with a specified temperature can be expressed in terms

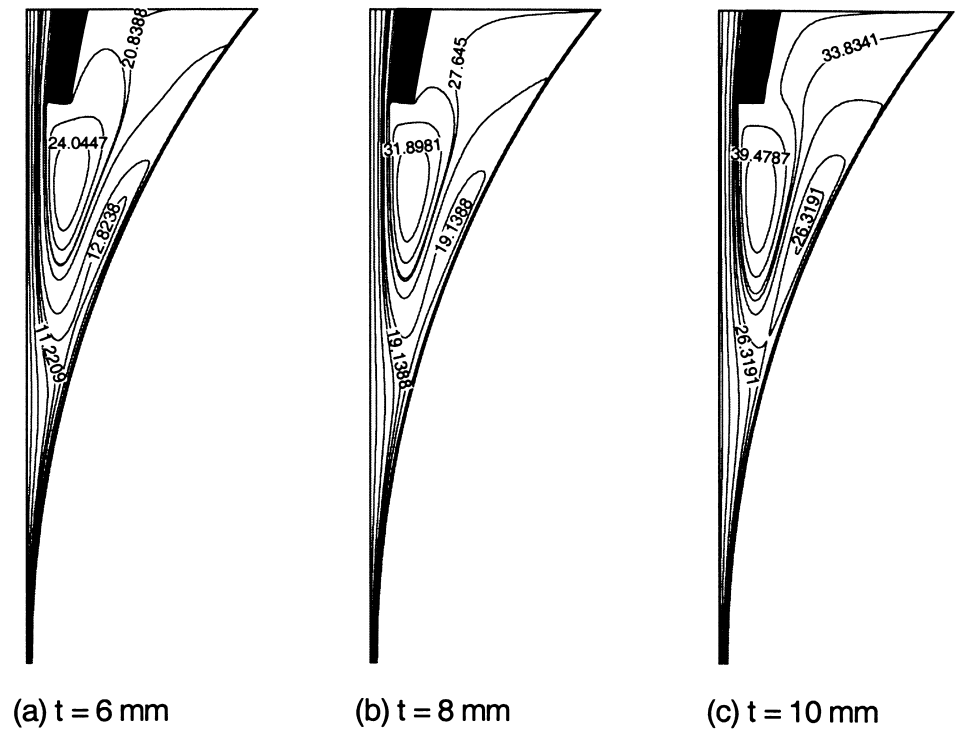


Fig. 5. Streamlines for various gap thicknesses of Type A: (a) $t = 6$ mm, (b) $t = 8$ mm, (c) $t = 10$ mm.

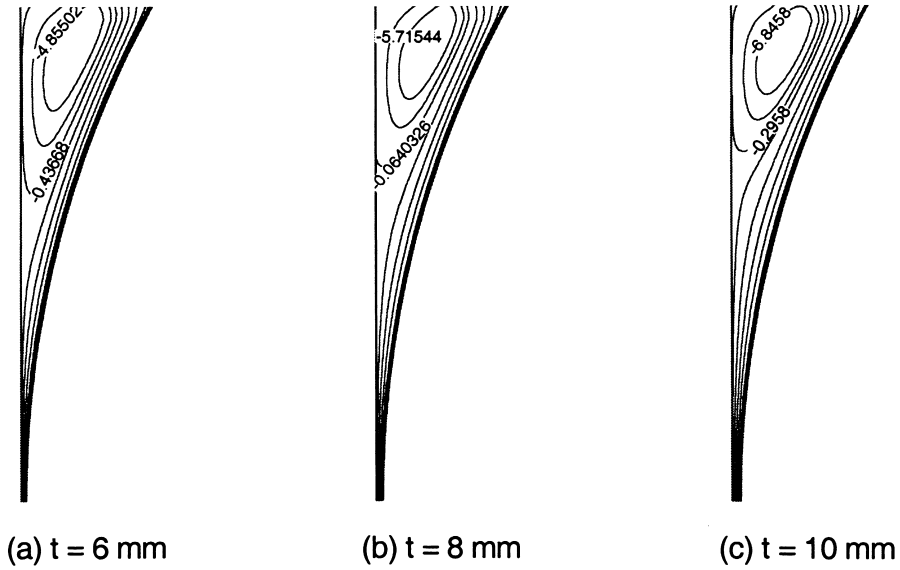


Fig. 6. Streamlines for various gap thicknesses of Type B: (a) $t = 6$ mm, (b) $t = 8$ mm, (c) $t = 10$ mm.

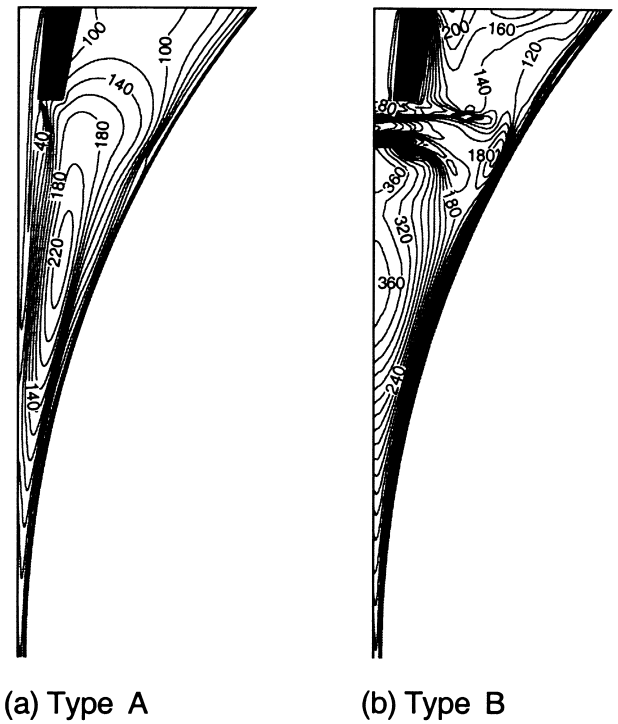


Fig. 7. Non-dimensional turbulent viscosity for gap thickness of 10 mm: (a) Type A, (b) Type B.

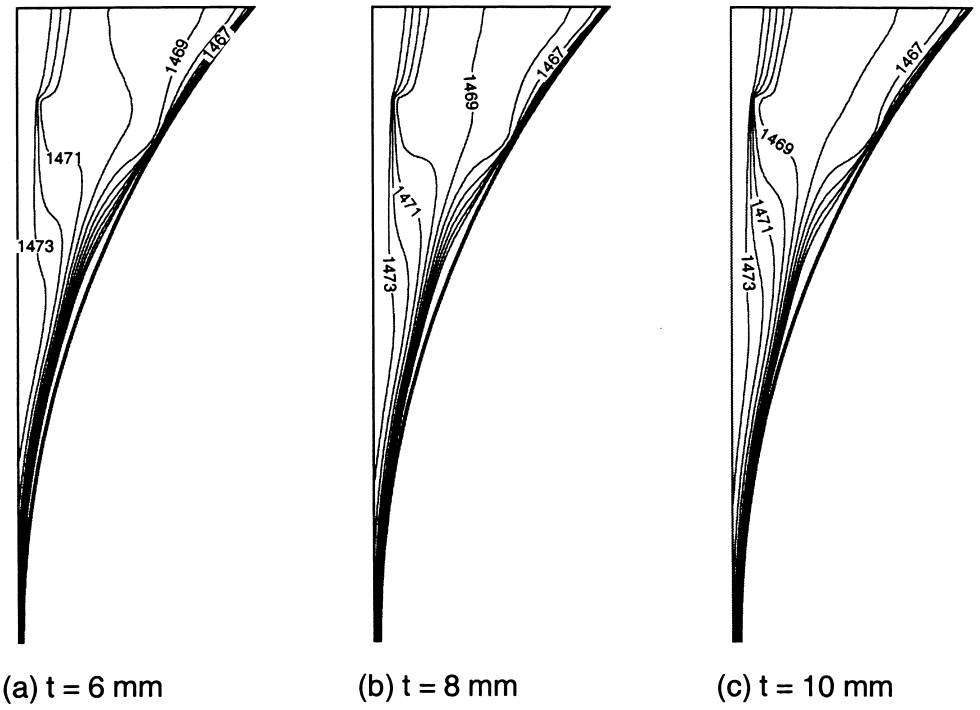


Fig. 8. Isotherms for various gap thicknesses of Type A: (a) $t = 6$ mm, (b) $t = 8$ mm, (c) $t = 10$ mm.

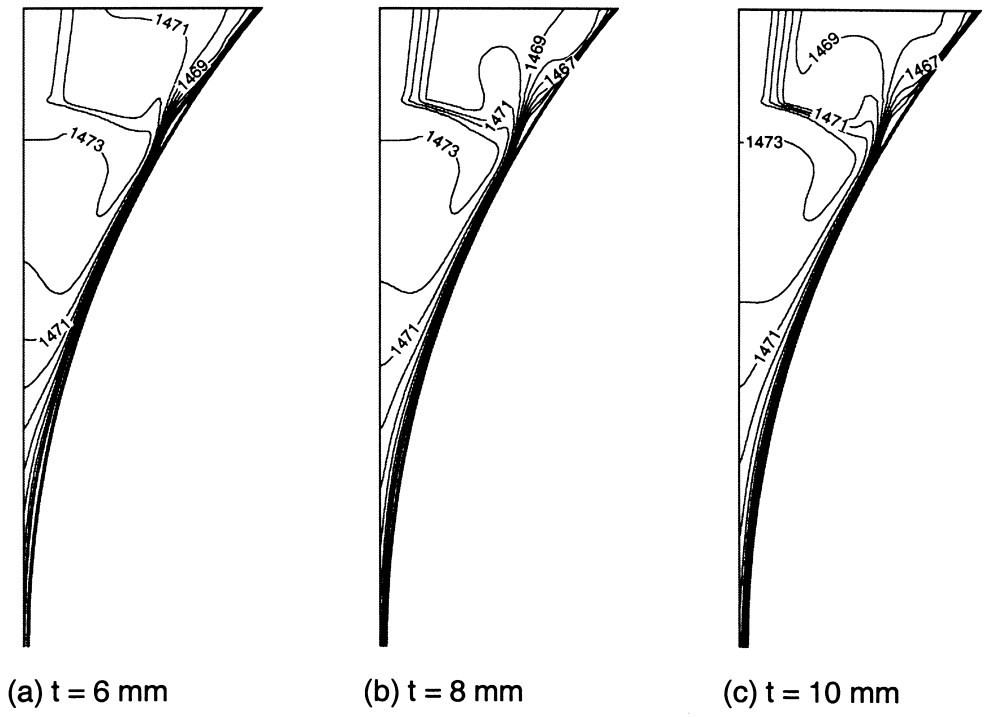


Fig. 9. Isotherms for various gap thicknesses of Type B: (a) $t = 6$ mm, (b) $t = 8$ mm, (c) $t = 10$ mm.

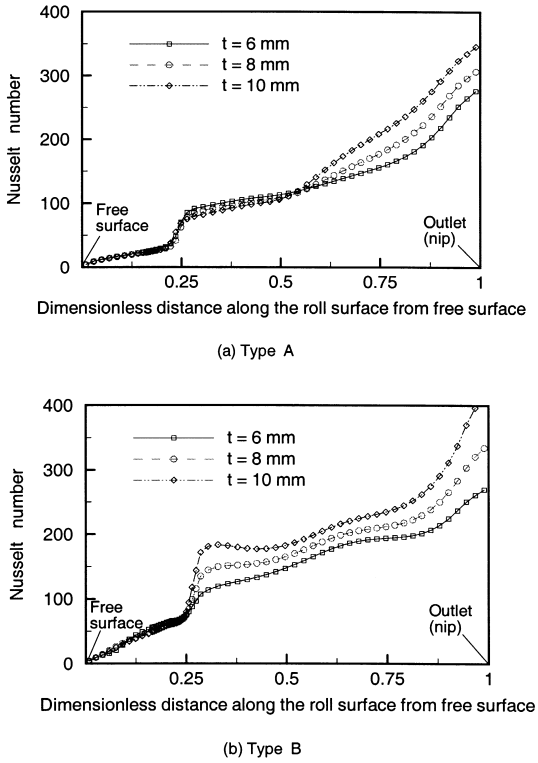


Fig. 10. Variation of Nusselt number along the roll surface for different gap thicknesses: (a) Type A, (b) Type B.

of the local Nusselt number ($Nu_1$), which is as follows:

$$Nu_1 = \frac{hs}{K} = \left( \frac{s}{(T_{in} - T_r)} \frac{\partial T}{\partial n} \right)_r \quad (13)$$

In order to investigate the effects of different gap thicknesses and melt-feed-types on the characteristics ($Nu_1$ distribution) of the heat transfer at the roll surface, the effects of the different gap thicknesses on the variation of $Nu_1$ for nozzle Types A and B at the roll surface are shown in Fig. 10 with respect to the non-dimensional distance from the free surface along the roll surface. As shown in Fig. 10, the Type B nozzle has larger values of $Nu_1$ than Type A for equal gap thicknesses over most of the roll surface. Because of this it is found that the temperature gradient on the roll surface for Type B is higher than the one for Type A. The abrupt change of $Nu_1$ observed around the non-dimensional distance of 0.25 is due to the fact that for Type A (Fig. 5), a part of the flow toward the free surface from the pool center impinges on the shear flow formed by the rotating rolls. For Type B (Fig. 6), the melt fed from the nozzle impinges directly on the roll surface, resulting in an increase in the temperature gradient in this region. Up to the outlet (nip) from the lower part of the roll surface, a slightly more rapid increase in $Nu_1$ as compared to that around the middle of the roll surface appears. This tendency, appearing close to the outlet, is caused by the fact that the strongly dominant turbulent flow, resulting from the reduction of the cross-sectional area of flow in the downstream section of the wedge-shaped pool, makes the temperature boundary layer thinner, resulting in an increase in $Nu_1$. The average heat transfer coefficient estimated from the local Nusselt number along the roll surface in Fig. 10 is about $2.0 \times 10^4$ (W/m$^2$/K).

## 4. Conclusions

In this study of twin-roll strip casting processes, in conjunction with the feed of molten steel through a submerged nozzle into a wedge-shaped pool using the vertical slit entry and bifurcated slit entry nozzle-types, respectively, an investigation of the coupled turbulent flow and heat transfer has been conducted. From the above numerical simulations, the following conclusions can be made:

1. For the feed of melt through a submerged nozzle, the Type A and B nozzles show two and three recirculating flow regions, respectively. The velocity vectors obtained in this study for a submerged nozzle were shown to be small in relation to the overall velocity when the velocities near the free surface were compared to those of Seyedein and Hasan [15] for a non-submerged nozzle. Therefore, the use of a submerged nozzle may be beneficial to the stabilization of the free-surface zone.
2. The results for the Type B nozzle provide slightly larger velocities and higher temperatures at the free surface, in comparison to those for the Type A nozzle. Therefore, it is expected that the Type B nozzle will have advantages over the Type A nozzle for the prevention of the skull formation at the free surface level.
3. For equal gap thicknesses, the Type B nozzle has larger values of $Nu_1$ over most of the roll surface, than those of Type A. An increase in the gap thickness leads to the movement of the isotherms toward the nozzle in the upper mid-pool region. In addition, the increase of $Nu_1$ in the downstream section with the reduction of the cross-sectional area of flow was noticeable in comparison to the upstream section of the wedge-shaped pool. The average heat transfer coefficient estimated from the local Nusselt number along the roll surface is about $2.0 \times 10^4$ (W/m$^2$/K).

## Acknowledgements

Woo-Seung Kim greatly acknowledges the financial

support from the LG Yonam Foundation for his sabbatical leave to North Carolina State University.

## References

[1] H. Jones, Rapid Solidification of Metals and Alloys, The Institution of Metallurgists, London, 1982.
[2] M. Cygler, M. Wolf, Continuous strip and thin slab casting of steel, Iron Steelmaker 13 (8) (1986) 27–33.
[3] L.L. Teoh, Technological developments in continuous thin slab and strip casters, Iron Steel Engineering 65 (12) (1988) 34–40.
[4] A.V. Kuznetsov, Numerical investigation of the macrosegregation during thin strip casting of carbon steel, Numerical Heat Transfer (Part A) 33 (1998) 515–532.
[5] A.V. Kuznetsov, Investigation of the coupled heat transfer, fluid flow and the solute transport during the strip casting process, International Journal of Heat and Mass Transfer 40 (12) (1997) 2949–2961.
[6] T.W. Clyne, A. Garcia, The application of a new solidification heat flow model to splat cooling, Journal of Materials Science 16 (6) (1981) 1643–1653.
[7] K. Miyazawa, J. Szekely, A mathematical model of the splat cooling process using the twin-roll technique, Metallurgical Transactions 12A (1981) 1047–1057.
[8] K. Miyazawa, T. Mizoguchi, N. Nakamura, T. Ohashi, The formation of thin steel strip in a laboratory scale twin-roll casting, in: Sahai et al. (Eds.), Casting of Near Net Shape Products, Proceedings of International Symposium, Honolulu, Hawaii, 1988, pp. 629–643.
[9] T. Saitoh, H. Hojo, H. Yaguchi, C.G. Kang, Two-dimensional method for twin-roll continuous casting, Metallurgical Transactions 23B (1989) 381–390.
[10] A. Mo, S.H. Hoydal, Mathematical modeling of temperature, melt flow, deformation and stress in aluminum twin roll casting, in: T.S. Piwonka, V. Voller, L. Katgerman (Eds.), Modeling of Casting, Welding and Advanced Solidification Processes VI, The Mineral, Metals and Material Society, New York, 1993, pp. 671–677.
[11] M.Y. Ha, K. Kim, K.C. Kim, S.W. Lee, Transient analysis of thermo-fluid phenomena in twin-roll continuous casting, International Journal of Heat and Mass Transfer 37 (14) (1994) 2059–2068.
[12] Y.D. Kim, C.G. Kang, A finite element heat transfer analysis with coupling of roll and molten metal in direct rolling process, Transactions KSME (Part B) 18 (4) (1994) 946–957 (in Korean).
[13] J.D. Hwang, H.J. Lin, W.S. Hwang, C.T. Hu, Numerical simulation of metal flow and heat transfer during twin roll casting, ISIJ International 35 (2) (1995) 170–177.
[14] C.G. Kang, Y.D. Kim, S.W. Lee, A solidification and cooling roll deformation analysis considering thermal flow in twin roll strip continuous casting process, in: E.F. Matthys, W.G. Trucker (Eds.), Melt Spinning Strip Casting and Slab Casting, TMS Annual Meeting in Anaheim, CA, February 4–8, 1996, pp. 65–87.
[15] S.H. Seyedein, M. Hasan, Numerical simulation of turbulent flow and heat transfer in the wedge-shaped liquid metal pool of a twin-roll caster, Numerical Heat Transfer (Part A) 31 (1997) 393–410.
[16] B.E. Launder, B.I. Sharma, Application of the energy dissipation model of turbulence to the calculation of flow near a spinning disc, Lett. Heat Mass Transfer 1 (1974) 131–138.
[17] K.Y.M. Lai, M. Salcudean, S. Tanaka, R.I.L. Guthrie, Mathematical modeling of flows in large tundish systems in steelmaking, Metallurgical Transactions 17B (1986) 449–459.
[18] S.V. Patankar, Numerical Heat Transfer and Fluid Flow, Hemisphere, Washington, DC, 1980.